

Welded plate and T-stub tests and implications on structural behavior of moment frame connections

P. Dong[†] and T. Kilinski[‡]

Center for Welded Structures Research, Battelle Memorial Institute, Columbus, OH 43201, USA

Abstract. A series of tests on simple-welded plate specimens (SWPS) and T-stub tension specimens simulating some of the joint details in moment frame connections were conducted in this investigation. The effects of weld strength mismatch and weld metal toughness on structural behavior of these specimens were considered under both static and dynamic loading conditions. Finite element analyses were performed by taking into account typical weld residual stress distributions and weld metal strength mismatch conditions to facilitate the interpretation of the test results. The major findings are as follows: (a) Sufficient specimen size requirements are essential in simulating both load transfer and constraint conditions that are relevant to moment frame connections, (b) Weld residual stresses can significantly elevate stress triaxiality in addition to structural constraint effects, both of which can significantly reduce the plastic deformation capacity in moment frame connections, (c) Based on the test results, dynamic loading within a loading rate of 0.02 in/in/sec, as used in this study, premature brittle fractures were not seen, although a significant elevation of the yield strength can be clearly observed. However, brittle fracture features can be clearly identified in T-stub specimens in which severe constraint effects (stress triaxiality) are considered as the primary cause, (d) Based on both the test and FEA results, T-stub specimens provide a reasonable representation of the joint conditions in moment frame connections in simulating both complex load transfer mode and constraint conditions.

Key words: moment frame connections; finite element analysis; T-stub specimens; brittle fracture; stress triaxiality; residual stresses; joint constraint; weld strength mismatch.

1. Introduction

Brittle weld fracture in damaged moment frames in the 1994 Northridge Earthquake has been a major subject of investigation over the recent years. Various potential factors that could have contributed to the brittle fracture phenomenon have been investigated within a major collaborative program (e.g., see SAC 95-08, 1995). These include low temperature, low weld metal toughness, weld defects, etc. However, high stress triaxiality due to severe structural restraint conditions, residual stresses, weld strength mismatch effects on joint performance have not been investigated in detail.

For instance, there exists ample evidence that both joint constraint conditions and high residual stresses (Zhang and Dong 2000, Matos and Dodds 2000) can play a dominant role in the fracture process of moment frame connections. The design of typical welded moment resistant frame connections represents rather severe mechanical constraint conditions both during welding and in service, due to the presence of continuity plates. Consequently, high weld residual stresses are present. In addition, the

[†]Technical Director (dongp@battelle.org)

[‡]Principle Research Engineer

triaxiality of the residual stress state in these joints can be significant such that the anticipated plastic deformation capacity may not develop before the fracture driving force reaches its critical value, resulting in brittle fracture (Zhang and Dong 2000).

Within the SAC Steel Project (Dong *et al.* 1999a), a large number of static and dynamic tests were performed using welded wide-plate and T-stub specimens. In addition to detailed testing, the underlying mechanics associated with the behavior of the test specimens were analyzed using some of the advanced finite element methods (Dong 2000) by considering both weld residual stress effects and structural loading conditions. In this paper, the test specimen design requirements and test procedures are first described. The test results are then summarized. The analysis of the test results is then provided in light of the detailed finite element results. Finally, implications of the current test results on the mechanical performance of the moment frame joints are then discussed.

2. Approach

To facilitate the planning and interpretation of the mechanical and fracture mechanics testing, advanced finite element techniques for welded structures were used to quantify some of the welding and specimen design effects on joint behavior in the test specimens.

It is well known that constraint can have a significant effect on failure ductility of metals. Fig. 1 illustrates a typical failure locus of test data. Here we define constraint as σ_m/σ_{eq} with:

$$\sigma_m = (1/3)(\sigma_1 + \sigma_2 + \sigma_3)$$

$$\sigma_{eq} = \sqrt{(3/2)S_{ij}S_{ij}}$$

$$S_{ij} = \sigma_{ij} - \sigma_m$$

As seen in Fig. 1, the plastic strain at failure decreases (ductility decreases) as constraint increases. For base metal, the constraint varies throughout a structure and depends on a number of factors

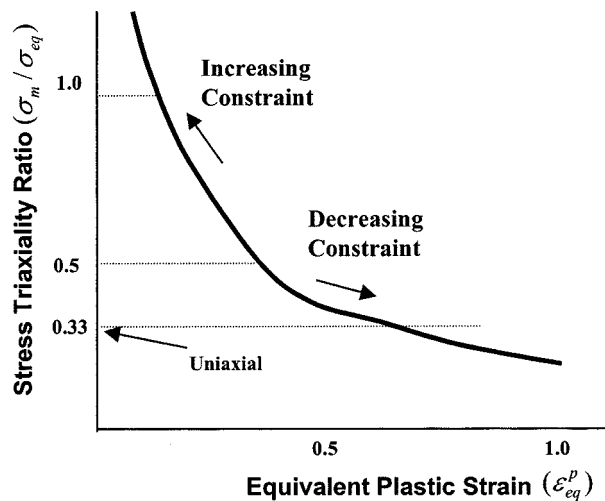


Fig. 1 Typical failure locus for metals as a function of joint constraint

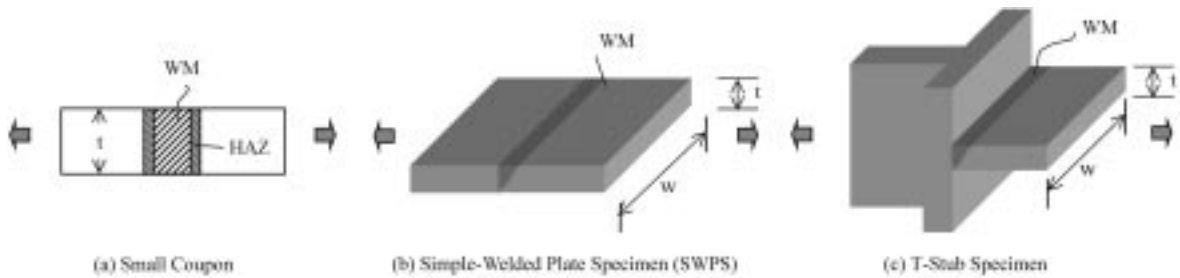


Fig. 2 Typical failure locus for metals as a function of joint constraint: (a) Small coupon-ASTM E8; (b) Wide plate specimens-simple welded plate specimens; (c) T-stub specimen

including geometry, loading mode, local stress state, residual stress state, and amount of plasticity, etc. To effectively interpret test results, it is essential that appropriate specimen design should be examined for investigating intended constraint conditions that are relevant in moment frame connections.

2.1. Rationale for specimen design

As shown in Fig. 2, small coupon specimens (ASTM E8) are typically used for testing base material (BM) and weld material (WM) stress-strain properties. By definition, the constraint effects are negligible so that uni-axial stress state can be reasonably assumed. Weld material behavior can be adequately estimated if the weld width is about the thickness of the base plate (Dong and Gordon 1992). However, it should be noted that plastic deformation capacity as well as fracture strength extracted from such specimens should only be interpreted as those under uniaxial conditions. To apply them in structural integrity assessment for complex structures such as moment frame connections, three dimensional stress state (i.e., stress triaxiality) must be considered, for instance, using finite element analysis.

To investigate experimentally such structural effects (or constraint effects), a wide plate specimen such as the one shown in Fig. 2b can be used. As discussed by Zhang and Dong (2000) and Dong *et al.* (1999a), both structural constraint (in width direction) and weld residual stress considerations suggests that the width to thickness ratio should be at least $w/t \geq 6$. This ensures that welding-induced residual stresses can be retained and that a high degree of constraint can be achieved at the mid-width of the specimens. As shown in Fig. 3, as the width of the specimen increases to $w/t = 6$ from that for E8 specimen, the equivalent plastic strain development at the heat-affected zone (HAZ) is significantly reduced under a given nominal loading level beyond yield. Once welding residual stresses are considered, the plastic deformation development is further delayed and reduced. To simulate both the complex load transfer mode and constraint conditions in moment frame connections, T-stub specimens were chosen in this study.

Therefore, in the present investigation, the small tensile coupons, e.g., ASTM E8 type (Fig. 2a), are used for uniaxial stress-strain curve characterization and provide negligible lateral constraint. The wide plate specimens (i.e., SWPS in Fig. 2b), with an adequate width ($w/t = 6$), can subject the middle section of the specimen width to plane-strain (high constraint) deformation conditions, and therefore, provide insight on structural failure behavior in regions of high constraint. In addition, T-stub specimens subjected to tension as shown in Fig. 2c provide a means for assessing load transfer (from the horizontal beam flange to the vertical column flange) effects on 3D stress-strain states at the joint. This paper investigates the effect of constraint on welded moment frame structures both experimentally and by performing a few selected finite element (FE) analyses.

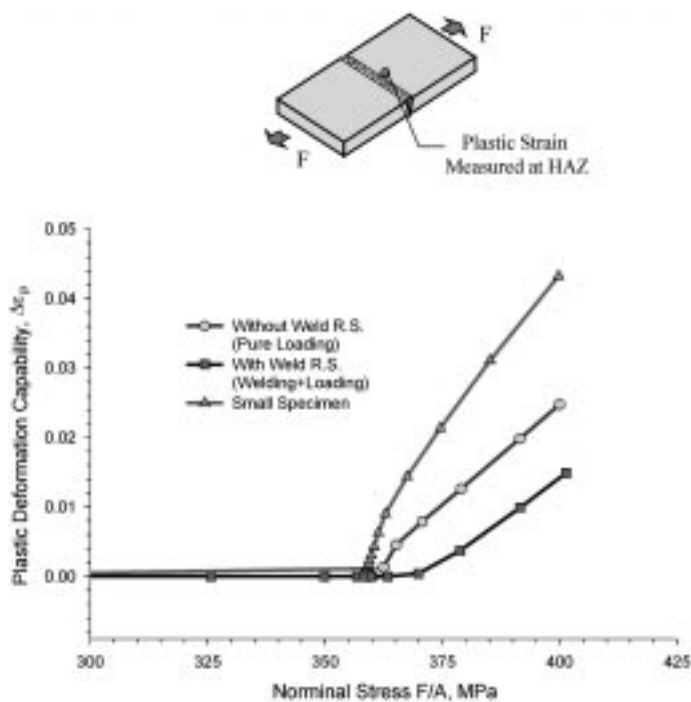


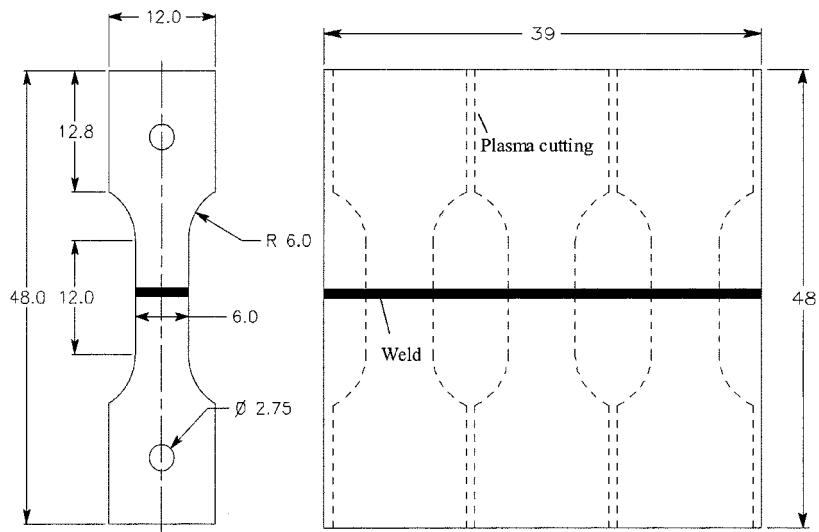
Fig. 3 Local plastic deformation capacity as a function of constraint and welding-induced residual stresses (BM: A36 with matched WM)

2.2. Specimen details, materials, and test procedures

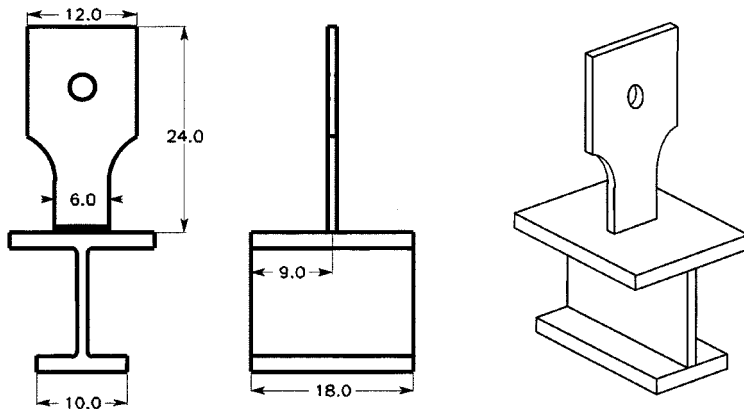
The dimension details and fabrication procedures for the wide plate (also referred as SWPS) and T-stub specimens are shown in Fig. 4. The BM and WM combinations for all test specimens are listed in Table 1. Four different base plate and two weld filler materials were used. The strength mismatches, defined as the ratio of uniaxial weld metal yield stress to uniaxial base material yield (or ultimate) stress, are listed in Table 1. The A572 Grade 60 plate with NR203 NiC weld filler metal, and HPS-70W plate and NR311 Ni weld filler are essentially matched materials in strengths. More details can be found in Dong *et al.* (1999a).

Testing on the SWPS plates was performed using a 4-post servo-hydraulic test frame with a rated capacity of 1,000,000 pounds. Load was measured using a load cell in series with the loading axis of the specimen. Displacement was measured using an LVDT internal to the hydraulic actuator. The T-stub specimens utilized the same fixturing for the “beam” segment of the specimen. Instrumentation for the tests consisted of load cell, actuator displacement (± 65 mm LVDT), average strain across the test weld in two locations (a 25 mm gage/50% extensometer and a 50 mm gage/50% extensometer), and remote strain in the base metal (25 mm gage/15% extensometer). Data was collected using LabTech Notebook[®] software running on a desktop PC equipped with a 16 channel, 16-bit D/A board.

Two types of tests were performed. One at a slow loading rate, which amounted to an applied strain rate of 0.00005 in/in/sec. The other, termed a fast rate, was 0.02 in/in/sec. It will be seen later that this ‘fast’ rate is actually not as ‘fast’ as one could expect in a dynamic earthquake event. Data was collected at 1 Hz for the slow rate tests, and at 1 kHz for the fast tests.



(a) SWPS Specimen (Unit: mm)



(b) T-Stub Specimen (Unit: mm)

Fig. 4 Specimen design and fabrication procedures: (a) SWPS specimen; (b) T-stub specimen

Table 1 Strength mismatch conditions for tests

	Plate			
	Yield (σ_y)		Ultimate (σ_{ult}) (ksi)	
Weld	A36	A572 Gr. 50	A572 Gr. 60	HPS 70W
σ_y / σ_{ult} (ksi)	42	54	60	85
	71	81	87	96
NR203 NiC	+55%	+20%	+8%	-24%
65/79	+11%	-2%	-9%	-18%
NR311 Ni		+50%	+35%	-5%
81/93		+15%	+7%	-3%

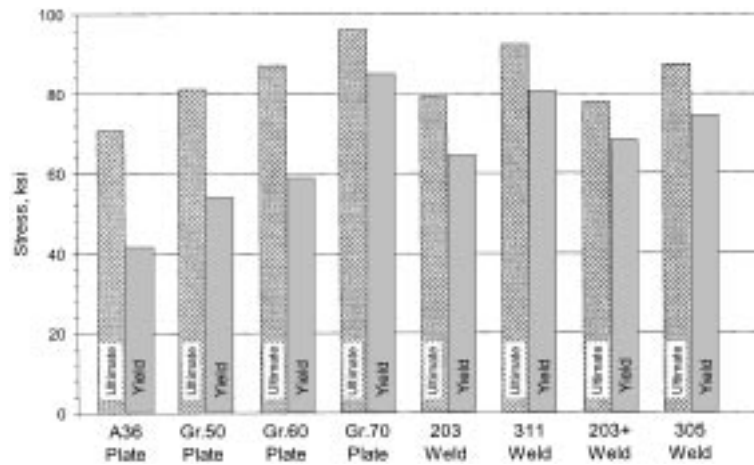


Fig. 5 Summary of small coupon (ASTM E8) test results

3. Test results and analysis

Small coupon tensile results are summarized in Fig. 5 in terms of both yield and ultimate tensile strengths. It should be noted that weld metal strength mismatch effects are typically characterized by WM to BM yield strength ratio since the dominant interaction mechanisms are in the form of plasticity between WM and BM, particularly from fracture mechanics viewpoint (Dong and Gordon 1992). This is also true if weld residual stresses are considered (Dong and Zhang 1999b). Furthermore, early studies (e.g., Dong and Gordon 1992) showed that for similar specimen sizes, yield strength mismatch effects can become significant for the current thickness (t) to weld width ratio (h) of unity, i.e., $h/t = 1$, if the mismatch ratio is above 20-25%. Therefore, the combinations of A572 Gr. 60/NR203 NiC and HPS 70W/NR311 Ni in Table 1 can be viewed approximately as matched conditions.

3.1. Simple welded plate specimens (SWPS)

By following the test procedures discussed earlier, a SWPS with A572 Gr. 70/NR 311Ni combination was first selected for some detailed instrumentation to gain initial insight on the structural behavior. As shown in Fig. 6, the overall load-displacement curve (with a gage length of 2") indicates that the nominal yield strength measured at 84 ksi from the SWPS reached the yield strength of the base material (HPS-70W), although with slightly under-matched weld metal (-5% in Table 1). The nominal failure stress (at peak load) was 96 ksi, with both necking and final failure in the base material about 1/4" away from the weld fusion line.

As discussed earlier, SWPS specimens are capable of providing some lateral constraint along the specimen width direction. Structural constraint generates stress triaxiality at mid-thickness or bi-axiality on the surface away from free edges. In Fig. 6b, the local strain development measured at the mid-length of the weld is plotted as a function of the applied nominal stress and is compared with a typical uniaxial stress-strain curve obtained for NR311 Ni weld metal. At a given loading level, at above 75 ksi, the delay in plastic strain development in SWPS can be attributed the presence of a bi-axial stress state. The difference can be more significant if a material point at the mid-thickness position is examined

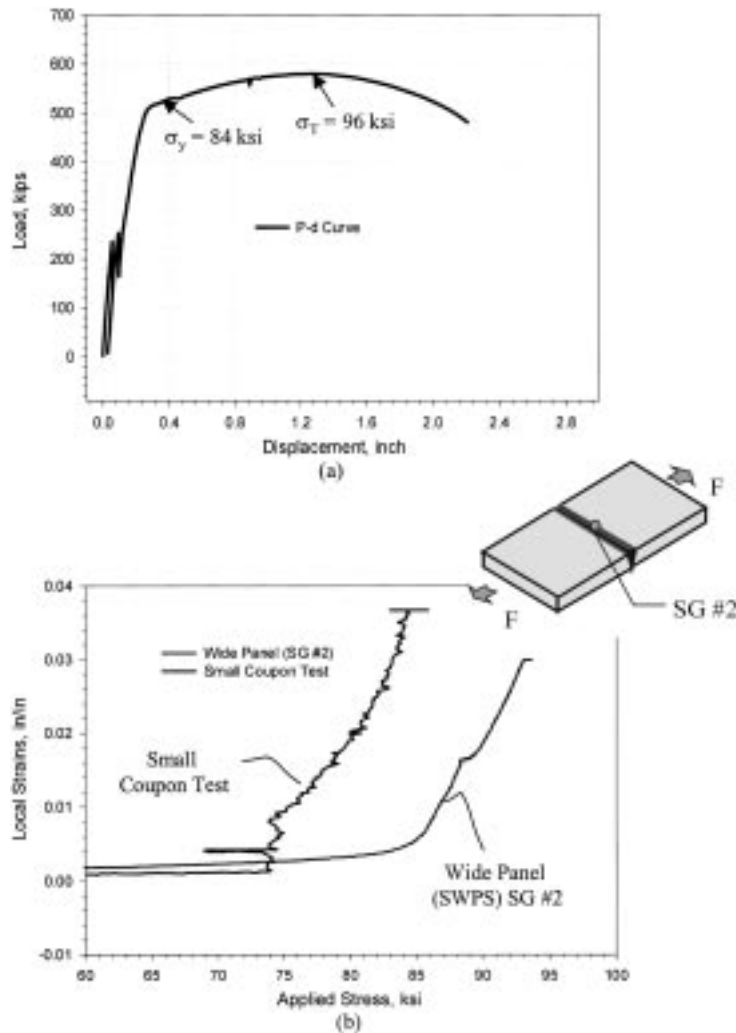


Fig. 6 Sample tensile test results-SWPS (BM: Gr. 70; WM: 311Ni, slow loading): (a) load vs displacement; (b) comparison of local strain development between SWPS and small coupon (E8)

due to the presence of tri-axial stress state. High stress triaxiality tends to delay or prevent plasticity development at a material point. Note that the uniaxial stress-strain curve used in Fig. 6b was obtained from the small coupon tests as shown in Fig. 5. The yield strength obtained from uniaxial tests for the same NR311 Ni weld metal was at about 80 ksi, slightly higher than the one used in Fig. 6b. Measured data tend to vary somewhat from test to test both in small coupon tests and in local strain measurements in SWPS, the general trend shown in Fig. 6b are correct and consistent with the finite element results indicated in Fig. 3.

The SWPS test results are summarized in terms of the measured nominal yield strength and ultimate strength in Fig. 7 for comparison. As far as global yield behavior observed from the load-displacement curves is concerned, the nominal yield strengths (e.g., F/A at yield load) of the SWPS specimens were all capable of reaching their respective BM yield strengths, even with under-matched WM yield strength

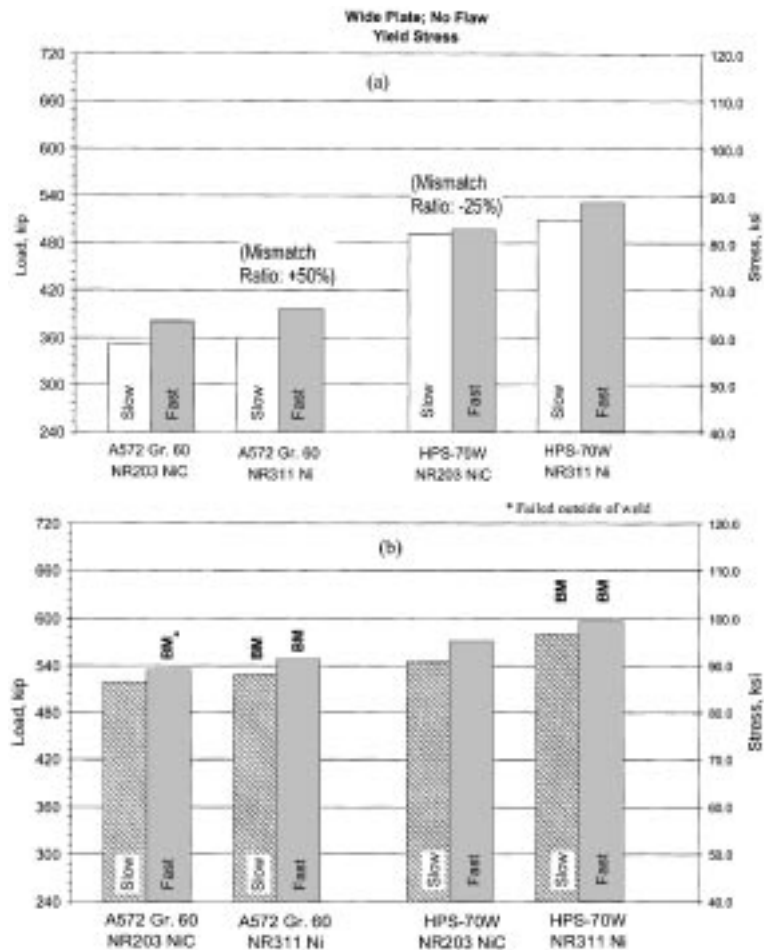


Fig. 7 Wide plate specimen test results: (a) load and nominal stress at yield; (b) peak load and peak nominal stress before failure (Note: BM indicates failure occurred outside of weld in base metal)

(about -25%) for the combinations HPS-70W/NR311 Ni. The “fast” loading rate tends to increase the measured yield strengths somewhat. The global ultimate strengths (corresponding to the peak load before final failure) showed a similar trend. However, final failures mostly occurred in the BM for matched and overmatched cases. It is worth noting that the ultimate (peak) load for the under-matched case (HPS-70W/NR203 NiC) still reached the nominal ultimate strength of the BM.

3.2. T-stub specimens

The detailed load-displacement results from T-stub specimens made of the A572 Gr. 60/NR203 NiC combination are shown in Fig. 8 under both slow and fast loading conditions. Again, some increase in nominal yield strength under fast loading conditions was observed. The majority of the fracture surface can be characterized as a brittle fracture due to significantly increased joint constraint conditions in the T-stub specimens to be discussed next.

The above observations can be further demonstrated using a 3D finite element model for the T-stub

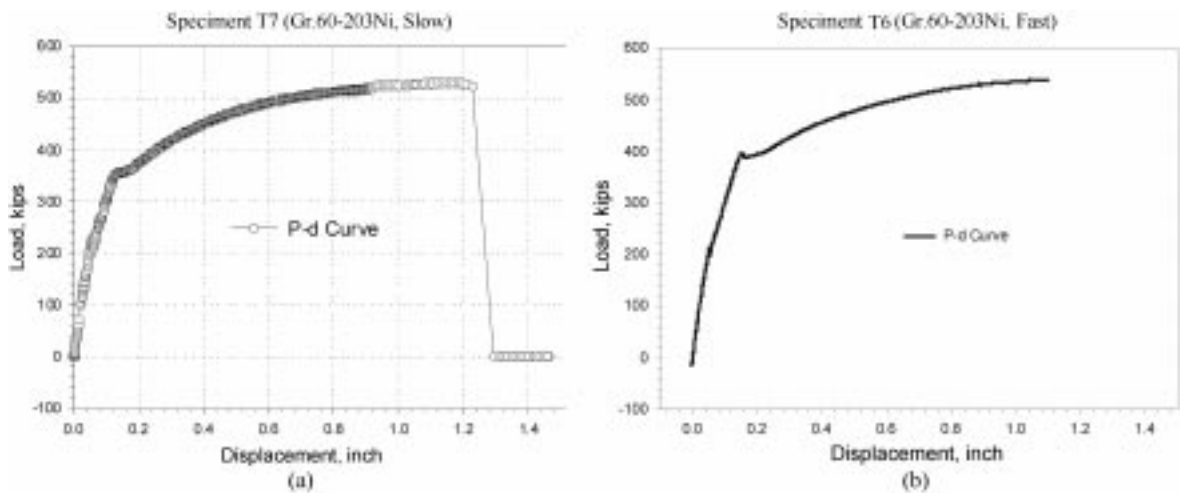


Fig. 8 Measured load-displacement curves for T-stub specimens (BM/WM: A572 Gr. 60/NR203 NiC): (a) Quasi-static loading; (b) Fast loading

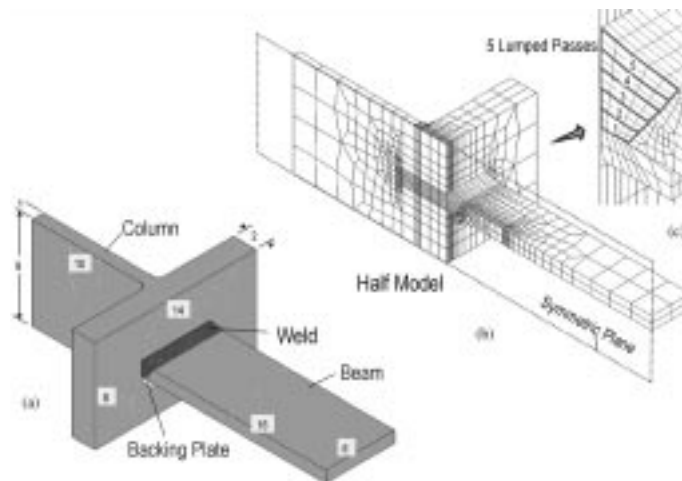


Fig. 9 Weld residual stress model for T-stub specimens: (a) specimen geometry, (b) finite element model, (c) weld pass details

specimen as shown in Fig. 9, where weld residual stress effects were included by considering a five lumped pass weld. The predicted residual stresses are summarized in Fig. 10. (The transverse residual stress distribution along the symmetry plane is rather similar to the one using 2D cross-section model as reported by Zhang and Dong (2000)). Note that near weld root, the residual stresses in all three directions have high magnitudes. The yield strength of the weld metal was assumed to be the same as the column material (A572 Gr. 50). The T-stub model was then used to simulate tension loading conditions used in the experiments.

Three locations were examined in detail, as shown in Fig. 11. The stress triaxiality normalized by the yield strength for A572 Gr. 50 ($(\sigma_1 + \sigma_2 + \sigma_3)/3\sigma_y$) as a function of remote nominal stress (F/A) are plotted in Fig. 11. As can be seen, the weld residual stresses played a significant role in the high stress

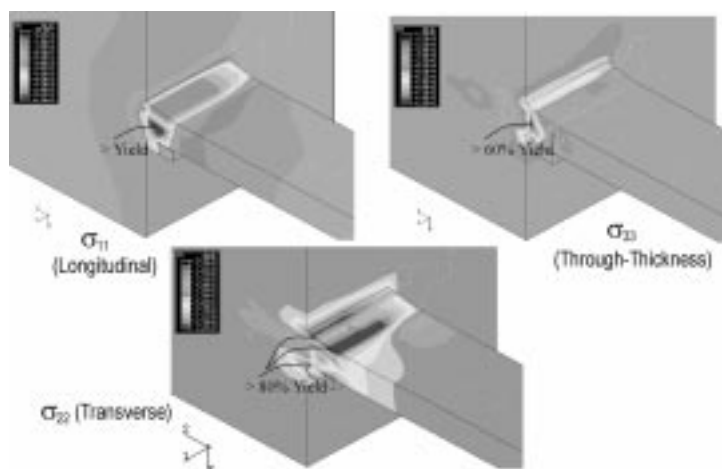


Fig. 10 Predicted residual stress distributions in T-stub specimen

triaxiality buildup within the weld region, e.g., Point #1 (Fig. 11a) and Point #2 (Fig. 11b). For instance, the stress triaxiality at Point #1 is already near unity (see the curve with circle symbols) even before loading is applied if weld residual stresses are considered. Away from the weld (Point 3), where weld residual stresses become insignificant (actually slightly compressive), the stress triaxiality increases linearly with the external loading. The triaxiality conditions remain essentially the same if the backing back is removed, as demonstrated in (Zhang and Dong 2000).

All T-stub test results are summarized in Fig. 12 in terms of the measured nominal yield and ultimate strengths. The fast loading rate tends to increase the measured yield strengths (Fig. 12a). This trend is consistent with SWPS results as shown in Fig. 7. Their overall effects on measured ultimate strength are less noticeable (Fig. 12b). However, a detailed visual examination of the fracture surfaces indicates that brittle fracture characteristics (relatively flat and shining portions of the surfaces) can be observed on the fracture surfaces of all five T-stub specimens (out of a total of six T-stub specimens tested) with final fracture within the weld. The resulting overall plastic deformation shown from the fracture surfaces is significantly less than those in SWPS specimens. Noticeable differences seem to exist in fracture behavior between the SWPS and T-Stub specimens either in terms of brittle fracture surface indications or final fracture paths. The significantly reduced plastic deformation associated with the final fracture can be attributed the triaxiality conditions that are more severe in the T-stub specimens (Fig. 11) than those in SWPS specimens.

4. Discussions

To contrast the difference in fracture mode between SWPS and T-stub specimens, Fig. 13 shows the fracture surfaces for cases with final fracture in the weld. It can be seen that with identical BM/WM combinations and loading conditions, there is a clear change in fracture mode from dominantly ductile (SWPS shown in Fig. 13a) to brittle* (T-stubs shown in Fig. 13b). The top three cases in Figure 13

*The failures were not truly brittle, but were clearly associated with much less plasticity compared with the SWPS specimen.

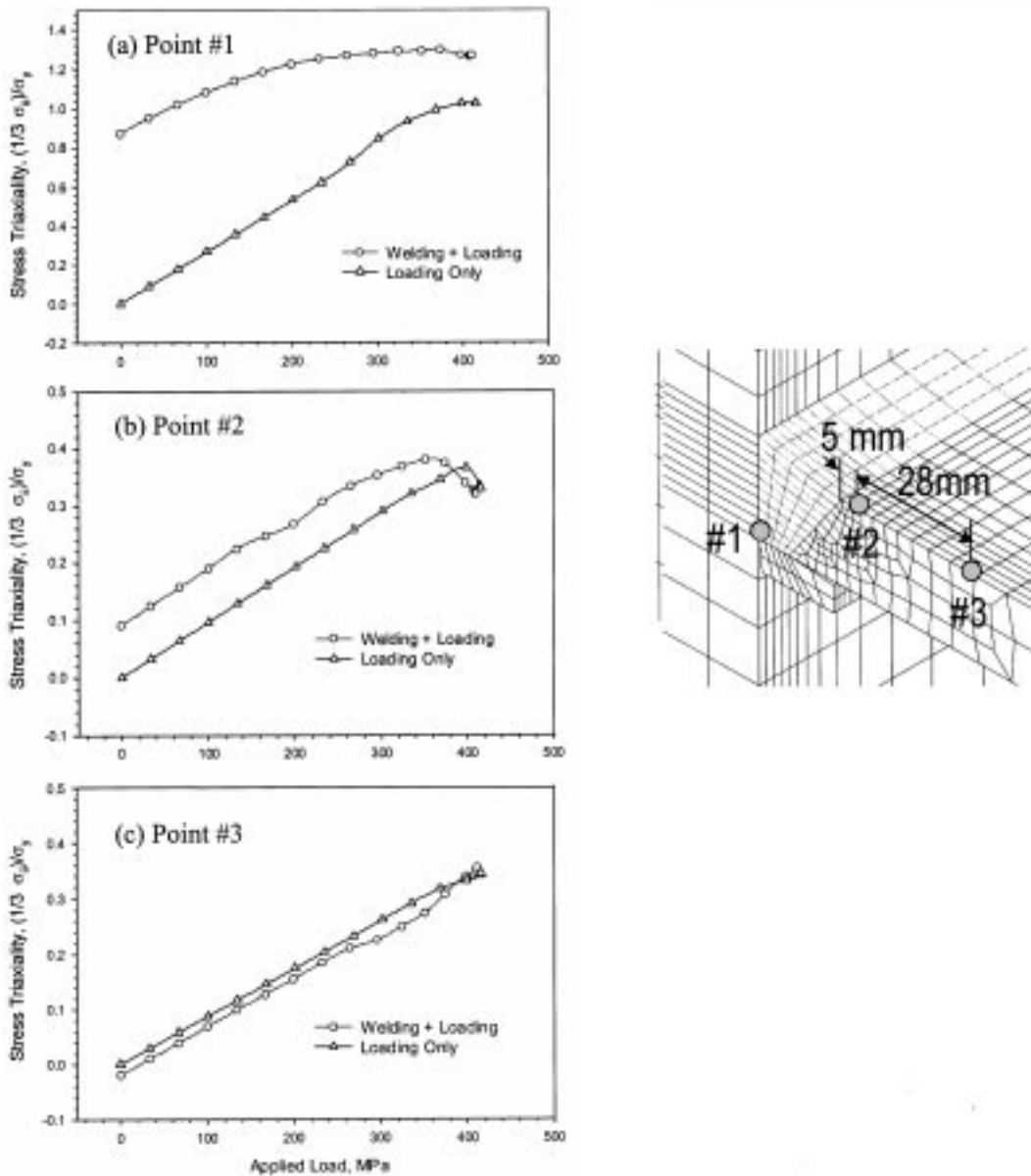


Fig. 11 Stress tri-axiality development in T-stub specimen as a function of remote loading and welding residual stresses: (a) point

represent matched yield strengths and the bottom case represents a weld under-matched case. This phenomenon can be attributed to the severe joint constraint conditions seen in T-stub specimens, regardless the weld metal strengths used. It is interesting to note that the brittle feature on the fracture surfaces in the T-stub specimens did not result in any noticeable reduction in the peak measured loads for most cases.

As discussed earlier, the greater the constraint present at potential failure positions, the lower the

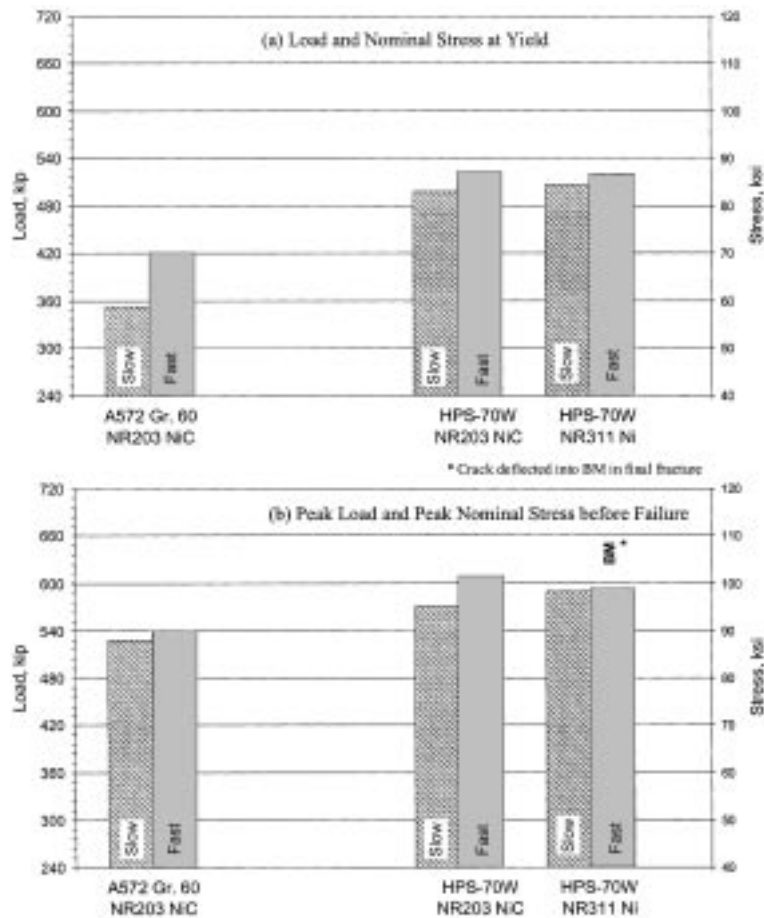


Fig. 12 T-stub test results: (a) load and nominal stress at yield; (b) peak load and peak nominal stress before failure.

ductility expected at failure. From the experimental results it was observed that the failures for the most highly constrained cases (T-stub) resulted in a more brittle fracture feature. The constraint comes from a number of sources. One source is the geometry of the T-stub specimen. The T-stub specimens are intended to simulate the conditions inherent in at a beam-column connection typically employed in steel building structures. For the case considered here (see Fig. 9), and typical in construction of many larger buildings, the column flange is thick and provides additional constraint to the beam flange compared with simply a plate (the beam thickness is also 1" or 25.4 mm).

Another additional source of constraint that often neglected is the weld induced residual stresses that develop in welded moment frames. The above observations are further supported by the 3D finite element results as shown in Figs. 10 and 11 for T-stub specimens, where weld residual stress effects were also considered by assuming a five-pass weld. The 3D residual stress distributions shown in Fig. 10 for T-stub specimens very much resemble those in a full 3D moment frame joint as shown in Fig. 14 (Zhang and Dong 2000). Although a direct stress triaxiality characterization for special moment frame connection joints was not performed here, it can be argued with a reasonable confidence that the joint

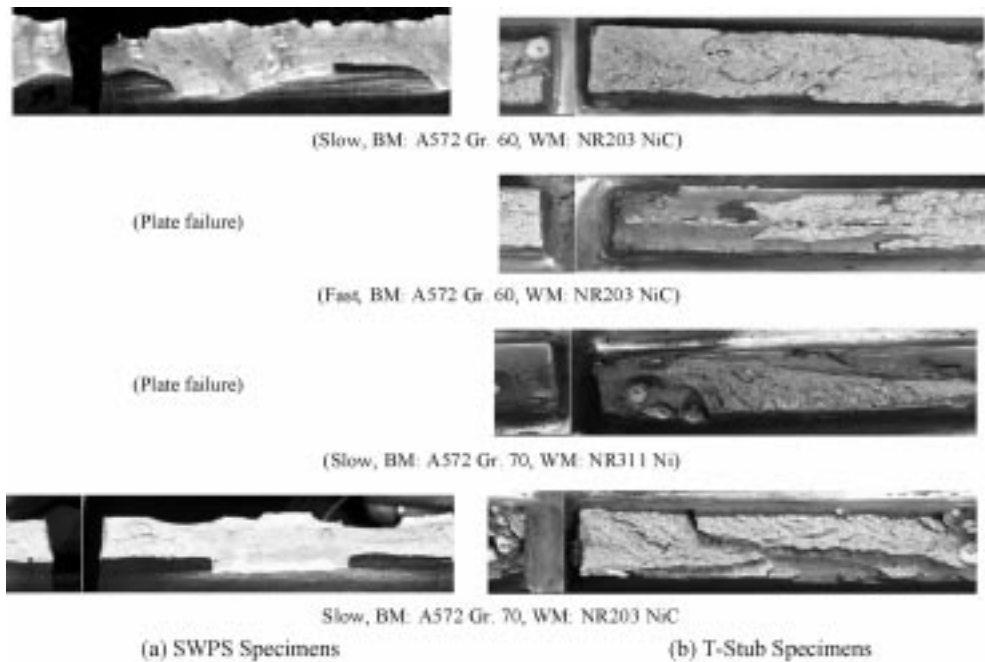


Fig. 13 Comparison of fracture surfaces between SWPS and T-stub specimens for failure in the weld

constraint conditions in T-stub specimens resemble more closely the actual constraint conditions in moment frame connections (Fig. 14). As such, the T-stub specimens should be more effective in reproducing the structural constraint conditions in actual moment frames than SWPS specimens.

The ultimate weldment strengths, as observed from the tests, were dominated by very complex interactions among WM, HAZ, and BM and final failure path. For the matched and overmatched cases (i.e., A572 Gr. 60/NR203 NiC, HPS-70W/NR311 Ni, and A572 Gr. 60/NR311 Ni), the ultimate weld strengths were largely dominated by final failure occurring in the base material in the SWPS specimens. For T-Stub specimens, however, most of the final failures (five out of six specimens) occurred in the weld. Furthermore, the fracture surfaces clearly indicate brittle fracture features in the five specimens.

One purpose of this paper was to investigate the potential failure modes in dynamic earthquake type loading conditions in moment frame structures. However, the test results indicated that loading rates effects were not significant within the “slow” (about 0.00001 in/in/sec) and “fast” (about 0.02/in/in/sec) loading rates, under specified test conditions. A consistent increase in both yield load and peak load before failure can be seen under the fast loading conditions. There is no clear trend identified in either failure location or fracture appearance between the two extreme loading rates within the same type of specimens.

It is well known that at high strain rates the yield strength of steel increases, and if the strain rates are high enough, premature fracture can result. As discussed earlier, the current test results showed that the peak loads before final fracture tend to increase in a consistent manner under fast load rate conditions. Charpy tests were also performed (see Dong *et al.* 1999). The CVN toughness is considerably lower in the A572 Grade 50 and 60 steels compared to the other steels and weld metals, even at temperatures

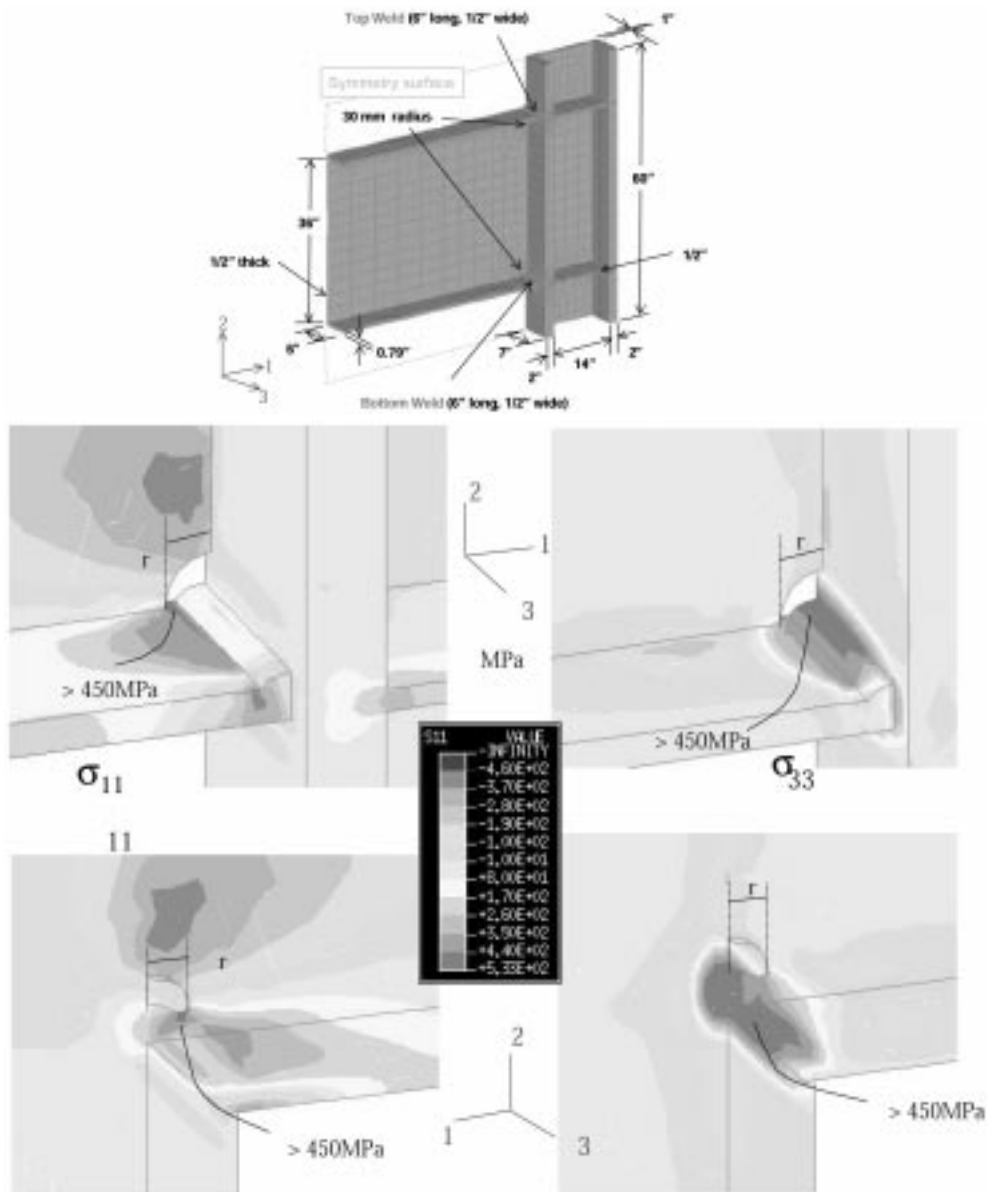


Fig 14. 3D Residual stress distributions in a moment frame joint

considerably higher than room temperature. One possible explanation is that the strain rates in the “fast” loading rate tests are actually much lower than those strain rates experienced in the Charpy tests, resulting in the apparent increase in failure loads. It is important to note that the strain rates experienced in the Charpy tests conducted in this study were approximately estimated at about 5-10 in/in/sec near the notch (Brust *et al.* 1993).

Some early work in studying nuclear piping systems under seismic loading conditions [e.g., see Brust *et al.* (1993), Marschall *et al.* (1994), Scott *et al.* (1994), and Rudland and Brust (1997)] examined the effects of loading rates on the tensile and fracture properties of nuclear steels. The slow loading rates

used in this Nuclear work were about the same level as used in the present study (strain rates were about .00005 in/in/sec). However, the fast loading rates in the present study were only .02 in/in/sec while the strain rates considered were up to 10 in/in/sec in the nuclear studies considering seismic loading. In Marschall (1994), it is observed that, for ductile stainless steels studied, loading rate has little effect on fracture loads. However, in the carbon steels studied, the fracture toughness of the steels was markedly decreased at the high loading rates (1 to 10 in/in/sec). These tests were conducted at light water reactor conditions of 288 C where the carbon steels were susceptible to dynamic strain aging. However, it may still be inferred that a marked decrease in fracture load (or fracture toughness) at a much higher high load rates (e.g., above 1 in/in/sec) may be expected for the SWPS and T-stub specimens here.

5. Conclusions

A series of SWPS and T-stub specimens have been tested and analyzed, particularly in terms of their structural constraint conditions. The major findings are as follows:

(a) Specimen size requirements are essential in simulating both load transfer mode, constraint conditions, as well as residual stress effects that are relevant to the structural performance of moment frame connections

(b) Weld residual stresses can significantly elevate stress triaxiality at both weld toe and weld root, resulting in reduced plastic deformation capacity in moment frame connections.

(c) Based on the test results, dynamic loading within a loading rate of 0.02 in/in/sec, as used in this study, premature brittle fractures were not observed, instead, a significant elevation of the yield strength can be clearly observed. Brittle fracture features can be clearly identified in T-stub specimens in which severe constraint effects (stress triaxiality effects) are considered as the primary cause.

(d) Detailed analyses on SWPS and T-stub specimens showed that T-stub specimens should provide a more representative constraint conditions in moment frame connections, while the SWPS specimens with $w/t = 6$ provide a simpler test configuration for incorporating some constraint and residual stress effects.

References

- Brust, F.W., et al., NUREG/CR-6098, (1993), "Loading rate effects on strength and fracture toughness of pipe steels used in task 1 of the IPIRG program", Prepared by Battelle for the US NRC.
- Brust, F.W., Zhang, J. and Dong, P., (1997a), "Pipe and pressure vessel cracking: the role of weld induced residual stresses and creep damage during repair", *Transactions of the 14th International Conference on Structural Mechanics in Reactor Technology (SMiRT 14)*, Lyon, France, **1**, 297-306.
- Brust, F.W., Dong, P. and Zhang, J., (1997b), "Crack growth behavior in residual stress fields of a core shroud girth weld", *Fracture and Fatigue*, H. S. Mehta, Ed., PVP. **350**, 391-406.
- Dong, P., (2000), "Modeling of weld residual stresses and distortions: computational procedures and applications", *Welding Research Council Bulletin*, No. 455, September, 1-11.
- Dong, P. and Gordon, J. R., (1992), "The effect of weld metal mismatch on the fracture behavior of center-cracked panels", *1992 ASME Pressure Vessels & Piping Conference*, June 21-25, 1992, New Orleans, Louisiana, PVP **241**, *Fatigue, Fracture, and Risk*, pp. 59-67.
- Dong, P., Kilinski, T., Zhang, J. and Brust, F.W., (1999a), "Effects of strength/toughness mismatch on structural and fracture behaviors in weldments", (Sub-Tasks 5.2.1 And 5.2.2), Battelle Final Report to SAC Steel Project.
- Dong, P. and Zhang, J., (1999b), "Residual stresses in strength-mismatched welds and implications on fracture

- behavior,” *Engineering Fracture Mechanics*, **64**, 485-505.
- Dong, P., Zhang, J. and Brust, F.W., (2000), “Fracture mechanics analysis of moment frame joints incorporating welding effects”, submitted for publications in ASCE Journal Civil Engineering Materials.
- Marschall, C.W., *et al.*, 1994, “Effect of dynamic strain aging on the strength and toughness of nuclear ferritic piping at LWR temperatures”, NUREG/CR-6226.
- Matos, C. and Dodds, R., (2000), “Modeling the effects of residual stresses on defects in welds of steel frame connections”, *Engineering Structures*, **22**(9), 1103-1120.
- Rudland, D.L, Brust, F., (1997), “The effect of cyclic loading during ductile tearing on the fracture resistance of nuclear pipe steels”, *Fatigue and Fracture Mechanics: 27*, ASTM STP 1296, R.S. Piascik, J.C. Newman, and N.E. Dowling Eds., American Society of Testing and Materials, 406-426.
- SAC 95-08, (1995), Background Report: Metallurgy, Fracture Mechanics, Welding, Moment Connections and Frame Systems Behavior, Prepared by the SAC Joint Venture for the Federal Emergency Management Agency, Report No. FEMA-288, Washington, D.C.
- Scott, P., Olson, R. and Wilkowski, G., (1994), “The IPIRG- 1 pipe system fracture tests experimental results in fatigue”, Flaw Evaluation, and Leak-Before-Break Assessments, ASME PVP **280**, 135-151.
- Zhang, J., Dong, P. and Brust, F.W., (1998), “Residual stress analysis and fracture assessment of welded joints in moment resistance frames”, *Proc. Int. Conf. on Advances in Computational Engineering Science*, Vol. II: *Modeling and Simulation Based Engineering*, Atluri, S.N., and ODonoghue, P.E., eds., 1894-1902.
- Zhang, J., Dong, P., F.W. Brust, and others, (1999), “Modeling of weld residual stresses in core shroud structures”, *Nuclear Engineering and Design*, **195**, 171-187.
- Zhang, J. and Dong, (2000), “Residual stresses in welded moment frames and effects on fracture”, *ASCE J. Struct. Eng.*, March, No. 3.

CC